

WAVEMOTH – FAST SPHERICAL HARMONIC TRANSFORMS BY BUTTERFLY MATRIX COMPRESSION

D. S. SELJEBOTN¹*Draft version February 18, 2022*

ABSTRACT

We present *Wavemoth*, an experimental open source code for computing scalar spherical harmonic transforms (SHTs). Such transforms are ubiquitous in astronomical data analysis. Our code performs substantially better than existing publicly available codes due to improvements on two fronts. First, the computational core is made more efficient by using small amounts of precomputed data, as well as paying attention to CPU instruction pipelining and cache usage. Second, *Wavemoth* makes use of a fast and numerically stable algorithm based on compressing a set of linear operators in a precomputation step. The resulting SHT scales as $O(L^2 \log^2 L)$ for the resolution range of practical interest, where L denotes the spherical harmonic truncation degree. For low and medium-range resolutions, *Wavemoth* tends to be twice as fast as *libpsht*, which is the current state of the art implementation for the HEALPix grid. At the resolution of the Planck experiment, $L \sim 4000$, *Wavemoth* is between three and six times faster than *libpsht*, depending on the computer architecture and the required precision. Due to the experimental nature of the project, only spherical harmonic synthesis is currently supported, although adding support for spherical harmonic analysis should be trivial.

Subject headings: Methods: numerical

1. BACKGROUND

The spherical harmonic transform (SHT) is the spherical analog of the Fourier transform, and is an essential tool for data analysis and simulation on the sphere. A scalar field $f(\theta, \phi)$ on the unit sphere can be expressed as a weighted sum of the spherical harmonic basis functions $Y_{\ell m}(\theta, \phi)$,

$$f(\theta, \phi) = \sum_{\ell=0}^{\infty} \sum_{m=-\ell}^{\ell} a_{\ell m} Y_{\ell m}(\theta, \phi). \quad (1)$$

The coefficients $a_{\ell m}$ contain the spectral information of the field, with higher ℓ corresponding to higher frequencies. In calculations the spherical harmonic expansion is truncated for $\ell > L$, and the spherical field represented by $O(L^2)$ grid samples. Computing the sum above is known as the *backward SHT* or *synthesis*, while the inverse problem of finding the spherical harmonic coefficients $a_{\ell m}$ given the field f is known as the *forward SHT* or *analysis*.

In order to compute an SHT, the first step is nearly always to employ a separation of sums, which we review in Section 2.3, to decrease the cost from $O(L^4)$ to $O(L^3)$. We will refer to codes that take no measures beyond this to reduce complexity as brute-force codes. Of these, HEALPix (Górski et al. 2005) is one very widely used package, in particular among CMB researchers.

Recently, the *libpsht* package (Reinecke 2011) halved the computation time with respect to the original HEALPix implementation, simply through code optimizations. As of version 2.20, HEALPix uses *libpsht* as the backend for SHTs. Other packages using the brute-force algorithm include S²HAT (Hupca et al. 2010; Szydlarski et al. 2011), focusing on cluster parallelization

and implementations on the GPU, as well as GLESP (Doroshkevich et al. 2005) and ssht (McEwen & Wiaux 2011), focusing on spherical grids with more accurate spherical harmonic analysis than what can be achieved on the HEALPix grid.

The discovery of Fast Fourier Transforms (FFTs) has been all-important for signal analysis over the past half century, and there is no lack of high quality commercial and open source libraries to perform FFTs with stunning speed. Unfortunately, the straightforward divide-and-conquer FFT algorithms do not generalize to SHTs, and research in fast SHT algorithms has yet to reach maturity in the sense of widely adopted algorithms and libraries.

The *libftsh* library (Mohlenkamp 1999) uses local trigonometric expansions to compress the spherical harmonic linear operator, resulting in a computational scaling of $O(L^{5/2} \log L)$ in finite precision arithmetic. SpharmonicKit (Healy et al. 2003) implements a divide-and-conquer scheme which scales as $O(L^2 \log^2 L)$. We comment further on these in Section 4.4. Other algorithms have also been presented but either suffer from problems with numerical stability, are impractical for current resolutions, or simply lack publicly available implementations (e.g., Suda & Takami 2002; Kunis & Potts 2003; Rokhlin & Tygert 2006; Tygert 2008, 2010).

We present *Wavemoth*², an experimental open source implementation of the algorithm of Tygert (2010). This algorithm has several appealing features. First, it is simple to implement and optimize. Second, it is inherently numerically stable. Third, its constant prefactor is reasonable, yielding substantial gains already at $L \sim 2000$. The accuracy of the algorithm is finite, but can be arbitrarily chosen. For any given accuracy, the computational scaling is $O(L^2 \log^2 L)$, but lowering the requested accuracy makes the constant prefactor smaller.

d.s.seljebotn@astro.uio.no

¹ Institute of Theoretical Astrophysics, University of Oslo, P.O. Box 1029 Blindern, N-0315 Oslo, Norway² <http://github.com/wavemoth>; commit 59ec31b8 was used to produce the results of this paper.

We stress that our work consists solely in providing an optimized implementation. While we review the basics of the algorithm in Section 3, Tygert (2010) should be consulted for details and proofs. We have focused in particular on the HEALPix grid, and use `libpsht` as our baseline for comparisons. However, all methods work equally well for any other grid with iso-latitude rings.

Section 2 reviews SHTs in more detail, as well as the computational methods that are widely known and used across all popular codes. Section 3 reviews the algorithm of Tygert (2010) and how we have adapted it to our purposes. Section 4 focuses on the high-level aspects of software development and provides benchmarks, while an appendix provides the low-level implementation details.

2. BASELINE ALGORITHMS

2.1. The spherical harmonic basis functions

We use the convention that points on the sphere are parameterized by a co-latitude $\theta \in [0, \pi]$, where 0 corresponds to the “north pole”, and a longitude $\phi \in [0, 2\pi)$. The spherical harmonic basis functions $Y_{\ell m}(\theta, \phi)$ can then be expressed in terms of the *associated Legendre functions* $P_{\ell}^m(z)$. Assuming $m \geq 0$, we have

$$Y_{\ell m}(\theta, \phi) = \sqrt{\frac{2\ell+1}{4\pi} \frac{(\ell-m)!}{(\ell+m)!}} P_{\ell}^m(\cos\theta) e^{im\phi} \quad (2)$$

$$\equiv \tilde{P}_{\ell}^m(\cos\theta) e^{im\phi},$$

where we define the *normalized associated Legendre function* \tilde{P}_{ℓ}^m . Our definition follows that of Press et al. (2007); the normalization differs by a factor of $\sqrt{1/2}$ from the one in Tygert (2010).

Note that while the spherical harmonics $Y_{\ell m}$ and the coefficients $a_{\ell m}$ are complex, \tilde{P}_{ℓ}^m is real for the argument range of interest. For negative m , the symmetry $Y_{\ell, -m} = (-1)^m Y_{\ell m}^*$ can be used, although this is only needed for complex fields. Wavemoth only supports real fields, which have spherical harmonic expansions obeying $a_{\ell m} = (-1)^m a_{\ell, -m}^*$.

2.2. Discretization and the forward transform

For computational work one has to assume that one is working with a band-limited signal, so that $a_{\ell m} = 0$ when $\ell > L$. The SHT synthesis is then given simply by evaluating equation (1) in a set of points on the sphere.

The opposite problem of computing $a_{\ell m}$ given $f(\theta_j, \phi_j)$, namely spherical harmonic analysis, is less straightforward. In the limit of infinite resolution, we have

$$a_{\ell m} = \int f(\theta, \phi) Y_{\ell m}^*(\theta, \phi) d\Omega, \quad (3)$$

where $d\Omega$ indicates integration over the sphere. This follows easily from the orthogonality property,

$$\int Y_{\ell m} Y_{\ell' m'}^* d\Omega = \delta_{\ell\ell'} \delta_{mm'}. \quad (4)$$

There is no canonical way of choosing sample points on the sphere. The simplest grid conceptually is the equiangular grid. Doroshkevich et al. (2005) and McEwen & Wiaux (2011) describe grids that carries the orthogonality property of the continuous spherical harmonics over

to the discretized operator. In contrast, the HEALPix grid (Górski et al. 2005) trades orthogonality for the property that each pixel has the same area, which is convenient for many operations in the pixel basis.

Independent of what grid is chosen, a natural approach to spherical harmonic analysis is to use a quadrature rule with some weights w_j , so that

$$a_{\ell m} = \sum_{j=1}^{N_{\text{pix}}} w_j f(\theta_j, \phi_j) Y_{\ell m}^*(\theta_j, \phi_j). \quad (5)$$

On the HEALPix grid the numerical accuracy of this approach is limited, but it is still the most common procedure.

Some real world signal analysis problems do not need the forward transform at all. In the presence of measurement noise in the pixel basis, one can argue that the best approach is not to pull the noise part of the signal into spherical harmonic basis at all. For instance, consider the archetypical CMB data model,

$$\mathbf{d} = \mathbf{Y}\mathbf{s} + \mathbf{n}, \quad (6)$$

where \mathbf{d} represents a vector of pixels on the sky with observed data (not necessarily the full sky), \mathbf{s} represents our signal of interest in spherical harmonic basis, and \mathbf{n} represents instrumental noise in each pixel. Spherical harmonic synthesis is denoted \mathbf{Y} ; note that equation (1) describes a linear operator and can be written $\mathbf{f} = \mathbf{Y}\mathbf{a}$.

If we now assume that \mathbf{s} and \mathbf{n} are Gaussian random vectors with vanishing mean and known covariance matrices \mathbf{S} and \mathbf{N} , respectively, then the maximum likelihood estimate of the signal is given by

$$\hat{\mathbf{s}} = (\mathbf{S}^{-1} + \mathbf{Y}^\dagger \mathbf{N}^{-1} \mathbf{Y})^{-1} \mathbf{Y}^\dagger \mathbf{N}^{-1} \mathbf{d}, \quad (7)$$

with $\hat{\mathbf{s}}$ in spherical harmonic basis. This system can be solved with reasonable efficiency by iterative methods. Note that we are here only concerned with the effect of \mathbf{Y} as a non-invertible projection, and that no spherical harmonic analysis is ever performed, only the adjoint synthesis. Thus, neither the non-orthogonality caused by the HEALPix grid, nor masking out large parts of the sky, is a concern. See Eriksen et al. (2008) and references therein for more details on this technique in the context of CMB analysis.

2.3. Applying the Fast Fourier Transform

The first step in speeding up the spherical harmonic transform beyond the $O(L^4)$ brute-force sum is a simple separation of sums. For this to work well, pixels must be arranged on a set of iso-latitude rings, with equidistant pixels within each ring. All grids in use for high-resolution data has this property.

We show the case for SHT synthesis; analysis can be treated in the same way. Starting from equation (1), we have, for pixel j within ring k , and with $z_k \equiv \cos\theta_k$,

$$f(\theta_k, \phi_{k,j}) = \sum_{m=-L}^L \left[\sum_{\ell=|m|}^L a_{\ell m} \tilde{P}_{\ell}^m(z_k) \right] e^{im\phi_{k,j}} \quad (8)$$

$$\equiv \sum_{m=-L}^L q_m(z_k) e^{im\phi_{k,j}},$$

where we introduce $q_m(z_k)$. Assuming that ring k contains J_k pixels, their equidistant longitude is given by

$$\phi_{k,j} = \phi_{k,0} + \frac{2\pi j}{J_k}. \quad (9)$$

Since e^{ix} has period 2π , and since $q_m(z_k) = 0$ whenever $|m| > L$, we find that

$$\sum_{m=-L}^L q_{k,m} e^{im\phi_{k,j}} = \sum_{j=0}^{J_k-1} \tau_j(z_k) e^{2\pi j i / J_k} \quad (10)$$

with

$$\tau_j(z_k) = \sum_{t=-\infty}^{\infty} q_{J_k t + j}(z_k) e^{i\phi_{k,0}(J_k t + j)}. \quad (11)$$

Thus one can phase-shift the coefficients $q_m(z_k)$ to match the ring grid, wrap around or pad with zeros, and perform a regular backward FFT. The symmetries of the spherical harmonic coefficients of a real field carry over directly to the Hermitian property of real Fourier transforms.

This separation of sums represents a first step in speeding up the SHT, and is implemented in all packages for high-resolution spherical harmonic transforms.

2.4. Legendre transforms and even/odd symmetry

The function $q_m(z)$ introduced in equation (8) is known as the (*Associated*) *Legendre transform of order m* ,

$$q_m(z_k) = \sum_{\ell=m}^L \tilde{P}_{\ell}^m(z_k) a_{\ell m}, \quad (12)$$

assuming $m \geq 0$. The following symmetry cuts the arithmetic operations required in a SHT in half, as long as the spherical grid distributes the rings symmetrically around the equator. For any non-negative integer n , the functions $\tilde{P}_{m+2n}^m(z)$ are even and $\tilde{P}_{m+2n+1}^m(z)$ are odd. We define q_m^{even} and q_m^{odd} so that q_m^{even} contains the even-numbered and q_m^{odd} the odd-numbered terms of equation (12), and so that

$$q_m(z) = q_m^{\text{even}}(z) + q_m^{\text{odd}}(z). \quad (13)$$

Then, since q_m^{even} and q_m^{odd} are weighted sums of even and odd functions, respectively, they are themselves even and odd, so that $q_m(-z)$ can be computed at the same time essentially for free,

$$q_m(-z) = q_m^{\text{even}}(z) - q_m^{\text{odd}}(z). \quad (14)$$

For spherical harmonic analysis, one uses the orthogonality property. Assuming $m \geq 0$,

$$\int \tilde{P}_{\ell}^m(z) \tilde{P}_{\ell'}^m(z) dz = \delta_{\ell\ell'}, \quad (15)$$

so that

$$a_{\ell m} = \int \tilde{P}_{\ell}^m(z) q_m(z) dz. \quad (16)$$

As discussed in Section 2.2, the resulting quadrature used in calculations can be exact or approximate, depending on the placement of the pixel rings. One can also in this case cut computation time in half by treating even and odd $\ell - m$ separately.

3. FAST LEGENDRE TRANSFORMS

As the Fourier transform part is essentially a solved problem, efforts to accelerate SHTs revolve around speeding up the Legendre transforms. Let us write equation (12) as

$$\mathbf{q} = \mathbf{\Lambda}^T \mathbf{a}, \quad (17)$$

where we leave m and the odd versus even case implicit. For a full SHT, such a product must be computed for each of $2(L+1)$ different $\mathbf{\Lambda}$ matrices. The backwards Legendre transform required for spherical harmonic analysis is similarly

$$\mathbf{a} = \mathbf{\Lambda} \mathbf{q}, \quad (18)$$

give or take a set of quadrature weights.

The idea of Fast Legendre Transform algorithms is to compute equations (17) and (18) faster than $O(LN_{\text{ring}})$. The approach of Tygert (2010) is to factor $\mathbf{\Lambda}$ as a product of block-diagonal matrices in a precomputation step, which can significantly reduce the number of elements in total. This technique is known as *butterfly compression*, and was introduced by Michielssen & Boag (1996). The accuracy of the compression is tunable, but even nearly loss-less compression with close to double precision accuracy is able to yield significant gains as the resolution increases. We review the algorithm below, but stress again that the reader should consult Tygert (2010) for the full details. The butterfly compression technique was introduced by,

3.1. The interpolative decomposition

The core building block of the compression algorithm is the Interpolative Decomposition (ID), described in Cheng et al. (2005). Assume that an $m \times n$ matrix \mathbf{A} has rank k , then the ID is

$$\mathbf{A} = \mathbf{A}^{(k)} \tilde{\mathbf{A}}, \quad (19)$$

The matrix $\mathbf{A}^{(k)}$, known as the *skeleton matrix*, consists of k columns of \mathbf{A} , whereas $\tilde{\mathbf{A}}$, the *interpolation matrix*, interpolates the eliminated columns from the ones that are preserved. Of course, k of the columns of $\tilde{\mathbf{A}}$ must form the identity matrix.

The ID is obviously not unique; the trick is to find a decomposition that is numerically stable. The algorithm of Cheng et al. (2005) finds an interpolation matrix $\tilde{\mathbf{A}}$ so that no element has absolute value greater than 2, all singular values are larger than or equal to 1, and the spectral norm is bounded by $\sqrt{4k(n-k)+1}$. The numerical precision of the decomposition is tunable, as the decomposition found by the algorithm satisfies

$$\|\mathbf{A} - \mathbf{A}^{(k)} \tilde{\mathbf{A}}\| \leq \sqrt{4k(n-k)+1} \sigma_{k+1} \quad (20)$$

where σ_{k+1} is the $(k+1)$ greatest singular value of \mathbf{A} . Implementing lossy compression is simply a matter of reducing the accuracy required of the IDs we use.

3.2. Butterfly matrix compression

We now use the ID recursively to factor the matrix $\mathbf{\Lambda}$. After applying p levels of compression, we have

$$\mathbf{\Lambda} = \mathbf{R} \mathbf{S}_p \mathbf{P}_{p-1} \mathbf{S}_{p-1} \cdots \mathbf{P}_2 \mathbf{S}_2 \mathbf{P}_1 \mathbf{S}_1, \quad (21)$$

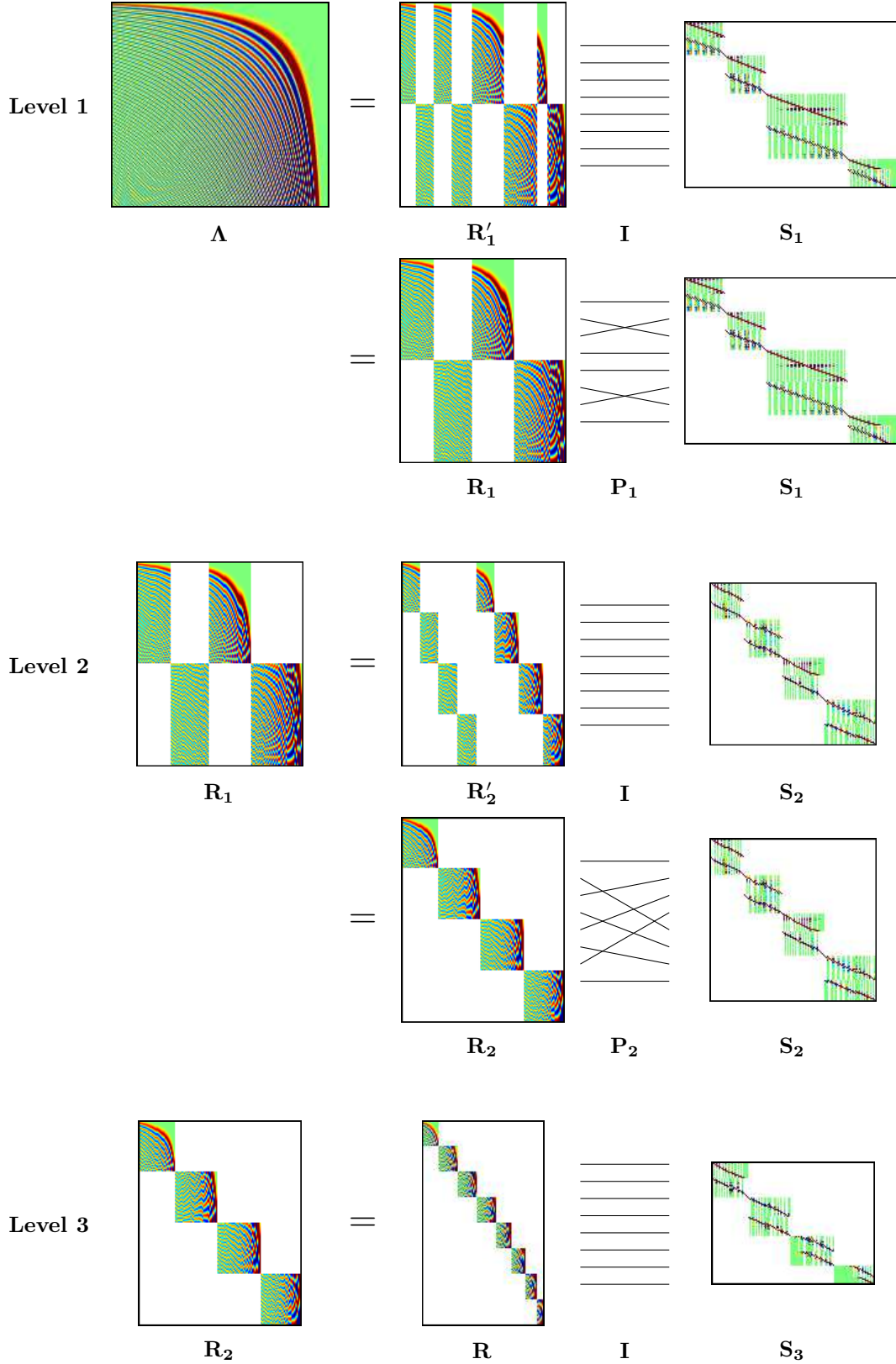


Figure 1. Illustration of the butterfly matrix compression scheme. On the first level, we use the Interpolative Decomposition to compress sub-blocks of the matrix Λ and produce the factorization $\Lambda = \mathbf{R}'_1 \mathbf{S}_1$, where all blocks in \mathbf{R}'_1 have full rank. We then proceed by permuting the columns of \mathbf{R}'_1 so that $\Lambda = \mathbf{R}_1 \mathbf{P}_1 \mathbf{S}_1$, in order to create new rank-deficient blocks. The contents of the \mathbf{S}_1 matrix is saved as precomputed data, while we carry \mathbf{R}_1 along for further compression on the next level. The algorithm continues in this fashion until the residual matrix \mathbf{R} only consists of a single diagonal of full-rank blocks. The final factorization becomes $\Lambda = \mathbf{R} \mathbf{S}_3 \mathbf{P}_2 \mathbf{S}_2 \mathbf{P}_1 \mathbf{S}_1$. The permutations involved are known in the FFT literature as *butterfly permutations*; the “butterfly” can be seen twice in the pattern of \mathbf{P}_1 .

where \mathbf{R} is a block-diagonal *residual matrix* containing elements that were not compressed, the \mathbf{S}_i are block-diagonal matrices containing compressed data, and the \mathbf{P}_i are permutation matrices. See Figure 1 for an illustration. The structure of the permutations are very similar to the *butterflies* used in FFT algorithms, hence the name of the compression scheme. In fact, if one lets \mathbf{S}_i contain a specific set of 2×2 -blocks on their diagonals one recovers the famous Cooley-Tukey FFT. In our case the blocks will be significantly larger, typically around 150×150 , although with much variation.

We start by partitioning $\mathbf{\Lambda}$ into 2^p column blocks. The number of levels p is mainly determined by the number of columns in the matrix, so that the column blocks all are roughly of the same predetermined width. In our case, 64 columns worked well.

We then split each block roughly in half horizontally, and compress each resulting block using the ID,

$$\begin{aligned} \mathbf{\Lambda} &= \begin{bmatrix} \mathbf{T}_{1,1} & \mathbf{T}_{1,2} & \cdots \\ \mathbf{B}_{1,1} & \mathbf{T}_{1,2} & \cdots \end{bmatrix} \\ &= \begin{bmatrix} (\mathbf{T}_{1,1}^{(k)} \cdot \tilde{\mathbf{T}}_{1,1}) & (\mathbf{T}_{1,2}^{(k)} \cdot \tilde{\mathbf{T}}_{1,2}) & \cdots \\ (\mathbf{B}_{1,1}^{(k)} \cdot \tilde{\mathbf{B}}_{1,1}) & (\mathbf{B}_{1,2}^{(k)} \cdot \tilde{\mathbf{B}}_{1,2}) & \cdots \end{bmatrix}, \end{aligned}$$

where the first subscript of each matrix refers to this being the first iteration of the algorithm. It is useful to write the above matrix as

$$\mathbf{\Lambda} = \begin{bmatrix} \mathbf{T}_{1,1}^{(k)} & \mathbf{T}_{1,2}^{(k)} & \cdots \\ \mathbf{B}_{1,1}^{(k)} & \mathbf{B}_{1,2}^{(k)} & \cdots \end{bmatrix} \begin{bmatrix} \tilde{\mathbf{T}}_{1,1} \\ \tilde{\mathbf{B}}_{1,1} \\ \tilde{\mathbf{T}}_{1,2} \\ \tilde{\mathbf{B}}_{1,2} \\ \ddots \end{bmatrix}.$$

We denote the right matrix \mathbf{S}_1 . It can not be further processed and its blocks are simply saved as precomputed data, making use of the fact that each block embeds the identity matrix in a subset of its columns.

The left matrix can be permuted and further compressed. For some permutation matrix \mathbf{P}_1 we have:

$$\begin{aligned} \mathbf{\Lambda} &= \begin{bmatrix} \mathbf{T}_{1,1}^{(k)} & \mathbf{T}_{1,2}^{(k)} & \cdots \\ \mathbf{B}_{1,1}^{(k)} & \mathbf{B}_{1,2}^{(k)} & \cdots \end{bmatrix} \mathbf{S}_1 \\ &= \begin{bmatrix} \mathbf{T}_{1,1}^{(k)} & \mathbf{T}_{1,2}^{(k)} & \cdots \\ \mathbf{B}_{1,1}^{(k)} & \mathbf{B}_{1,2}^{(k)} & \cdots \end{bmatrix} \mathbf{P}_1 \mathbf{S}_1. \end{aligned}$$

Then we join blocks horizontally, split them vertically, and compress each resulting block. For the top-left corner we have

$$\begin{bmatrix} \mathbf{T}_{1,1}^{(k)} & \mathbf{T}_{1,2}^{(k)} \end{bmatrix} = \begin{bmatrix} \mathbf{T}_{2,1} \\ \mathbf{B}_{2,1} \end{bmatrix} = \begin{bmatrix} (\mathbf{T}_{2,1}^{(k)} \cdot \tilde{\mathbf{T}}_{2,1}) \\ (\mathbf{B}_{2,1}^{(k)} \cdot \tilde{\mathbf{B}}_{2,1}) \end{bmatrix}. \quad (22)$$

Applying this to all blocks in the matrix, we get

$$\begin{aligned} \mathbf{\Lambda} &= \begin{bmatrix} (\mathbf{T}_{2,1}^{(k)} \cdot \tilde{\mathbf{T}}_{2,1}) & \cdots \\ (\mathbf{B}_{2,1}^{(k)} \cdot \tilde{\mathbf{B}}_{2,1}) & \cdots \\ & (\mathbf{T}_{2,2}^{(k)} \cdot \tilde{\mathbf{T}}_{2,2}) & \cdots \\ & (\mathbf{B}_{2,2}^{(k)} \cdot \tilde{\mathbf{B}}_{2,2}) & \cdots \end{bmatrix} \mathbf{P}_1 \mathbf{S}_1 \\ &= \begin{bmatrix} \mathbf{T}_{2,1}^{(k)} & & \mathbf{T}_{2,3}^{(k)} & \cdots \\ & \mathbf{B}_{2,1}^{(k)} & & \mathbf{B}_{2,3}^{(k)} & \cdots \\ & & \mathbf{T}_{2,2}^{(k)} & & \ddots & \cdots \\ & & & \mathbf{B}_{2,2}^{(k)} & & \cdots \end{bmatrix} \\ &\quad \cdot \begin{bmatrix} \tilde{\mathbf{T}}_{2,1} \\ \tilde{\mathbf{B}}_{2,1} \\ \tilde{\mathbf{T}}_{2,2} \\ \tilde{\mathbf{B}}_{2,2} \\ \ddots \end{bmatrix} \mathbf{P}_1 \mathbf{S}_1. \end{aligned}$$

And so the scheme continues. For each iteration the number of diagonals in the left matrix is halved, the number of blocks in each diagonal is doubled, and the height of each block is roughly halved. Eventually the left matrix consists only of a single diagonal band of blocks, and further compression is impossible. This becomes the residual matrix \mathbf{R} of equation (21).

The efficiency of the scheme relies on the non-trivial requirement that the $\mathbf{T}^{(k)}$ and $\mathbf{B}^{(k)}$ blocks are rank-deficient at every level of the algorithm. To get a handle on which matrices exhibit this behavior, we start with assuming the *rank property*, namely that any contiguous rectangular sub-block of $\mathbf{\Lambda}$, up to the numerical precision chosen, has rank proportional to the number of elements in the sub-block. That is, the rank does not depend on the location or shape of the block. Now, each time the butterfly algorithm joins two skeletons, such as $[\mathbf{T}_{1,1}^{(k)} \ \mathbf{T}_{1,2}^{(k)}]$ in equation (22), the resulting matrix has roughly $2k$ columns while spanning out a corresponding block of $\mathbf{\Lambda}$ of rank k . Therefore, half of the columns can be eliminated by applying the ID. Since the data volume is roughly halved at each compression level, and since \mathbf{S}_i at each level has $O(L)$ interpolative matrices of size roughly $k \times 2k = O(1)$, the resulting compressed representation of $\mathbf{\Lambda}$ has $O(L \log L)$ elements. See Tygert (2010) for a more detailed argument.

O'Neil et al. (2010) proves the rank property in the case of Fourier transforms and Fourier-Bessel transforms. It is however not proven in the case of associated Legendre functions $\tilde{P}_\ell^m(z)$. Figure 2 shows our results for resolutions up to $L \sim 130000$; we discuss these results further in Section 4.3.

3.3. Notes on interpolation

Tygert (2008) describes an elegant and exact interpolation scheme which, in the case of the HEALPix grid and $L = 2N_{\text{side}}$, reduces the number of required evaluation points for $q_m(z_k)$ by $2/3$. Although our conclusion was not to include this step in our code, we include a brief discussion in order to motivate our decision.

We focus on the even Legendre functions, the odd case is similar. Let n be an integer such that $L < m + 2n$.

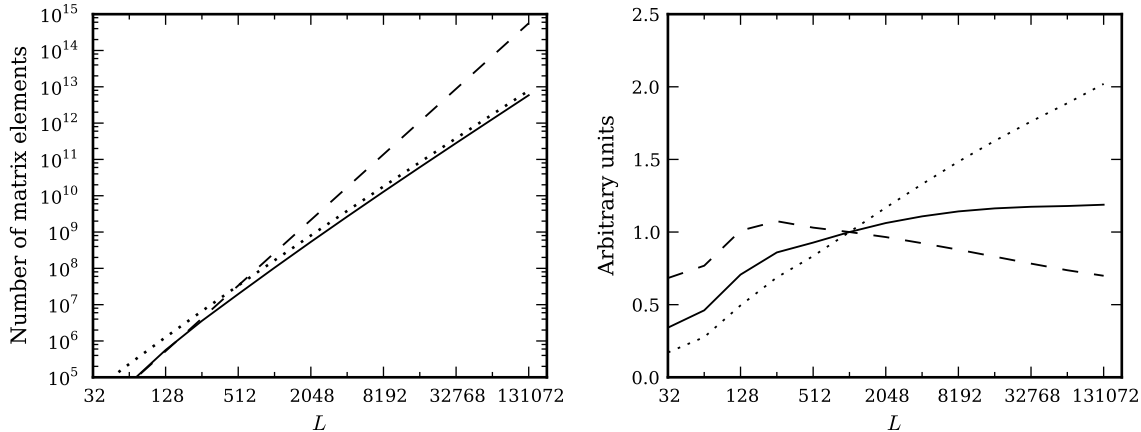


Figure 2. Efficiency of the butterfly compression scheme. *Left panel:* Estimated size of compressed data (solid) compared to uncompressed matrix size (dashed). A line proportional to $O(L^2 \log^2 L)$ (dotted) is shown for comparison. In each case we use a HEALPix grid with $N_{\text{side}} = L/2$. *Right panel:* A closer look on the computational scaling. The size of the compressed data is shown divided by $O(L^2 \log^3 L)$ (dashed), $O(L^2 \log^2 L)$ (solid) and $O(L^2 \log L)$ (dotted), using an arbitrary normalization.

The function $P_{m+2n}^m(x)$ has n roots in the interval $(0, 1)$, which we denote z_1, \dots, z_n . Now, assuming that we have evaluated q_m^{even} in these roots, we can interpolate to any other point $y \in (-1, 1)$ by using the formula

$$q_m^{\text{even}}(y) = \omega(y) \sum_{i=1}^n \frac{\gamma(z_i)}{y^2 - z_i^2} q_m^{\text{even}}(z_i), \quad (23)$$

for some precomputed weights $\omega(y)$ and $\gamma(z_i)$. The proof relies on the Christoffel-Darboux identity for the normalized associated Legendre functions (Tygert 2008; Jakob-Chien & Alpert 1997). The Fast Multipole Method (FMM) allows the computation of equation (23) for p points with operation count of order $O(p + n)$ rather than $O(pn)$. The FMM was originally developed for accelerating N -body simulations, but is here motivated algebraically. For more information about one-dimensional FMM we refer to Yarvin & Rokhlin (1999) and Dutt et al. (1996).

The reason we did not include this step in our code is that much of the interpolation is already embedded in the butterfly matrix compression. Consider for instance $N_{\text{side}} = 2048$, $L = 3N_{\text{side}}$ and $m = 2000$. The full matrix \mathbf{A} occupies 65 MiB when evaluated in the HEALPix co-latitude nodes, and only 49 MiB when evaluated in the optimal nodes as described above. However, after compression the difference is only 10.4 MiB versus 9.4 MiB. Thus the butterfly compression compensates, at least partially, for the over-sampling. Indeed, Martinsson & Rokhlin (2007) use a strongly related matrix compression technique to implement the FMM itself.

Interpolation also causes the precomputed data to become independent of the chosen grid and resolution. However, we found the constant prefactor in the FMM to be quite high, and including it only as a matter of convenience appears to be out of the question for our target resolutions. Since the FMM has a linear computational scaling, the question should be revisited for higher resolutions.

3.4. CPU and memory trade-offs

So far we have focused on reducing the number of floating point operations (FLOPs). However, during the

past decade the speed of the CPU has increased much more rapidly than the system memory bandwidth, so that in current multi-core computers it is easy to get in a situation where the CPUs are starved for data to process. When processing only one or a few transforms concurrently, the volume of the precomputed data is much larger than the volume of the maps being transformed, so that the limitation is moving the precomputed data over the memory bus, not processing power. Note that in the case of very many simultaneous transforms the problem is alleviated since the movement of precomputed data is amortized. Following in the footsteps of libpsht, and our own requirements in CMB analysis, we have restricted our attention to between one and ten concurrent transforms. While the butterfly algorithm probably performs well in the face of many concurrent transforms, it would require additional blocking and optimization beyond what we have implemented, so that movement of the working set in memory is properly amortized. Note that as each m is processed independently, the working set is only about $1/L$ of the total input.

The considerations above motivates stopping compression early, after a significant reduction in the floating-point operation count has been achieved, but before the size of the precomputed data becomes too large (see Figure 3). Butterfly compression has the convenient feature that the blocks in the residual matrix \mathbf{R} consists of contiguous slices from columns of \mathbf{A} . By orienting \mathbf{A} so that rows are indexed by ℓ and columns by z , the elements of the residual blocks can be computed on the fly from three-term recurrence formulas for the associated Legendre functions. We return to this topic in Section A.2.

As an example, consider $N_{\text{side}} = 2048$ and $m = 400$. The uncompressed matrix \mathbf{A} takes 64 MB in double precision. This can be compressed to 20% of the original size by using five levels of compression, with the uncompressed residual \mathbf{R} accounting for about 13% of the compressed data. If one instead stops after three levels of compression, then although the size of the compressed data has now grown to 24% of the original, 57% of this is made out of elements in \mathbf{R} . Since one only needs to store two elements for every column of 512 elements in \mathbf{R} and can generate the rest on the fly, stopping compres-

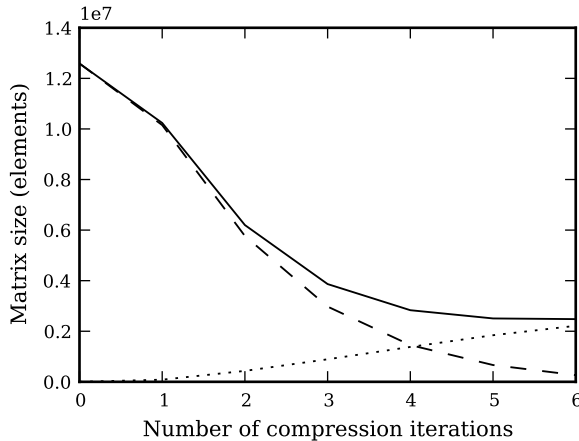


Figure 3. Effect of each level of butterfly compression. The size of the compressed data (solid) is the sum of elements in residual uncompressed blocks in \mathbf{R} (dashed) and the interpolation matrices \mathbf{S}_i (dotted). While \mathbf{R} can be generated on the fly during transforms, the \mathbf{S}_i needs to be stored as precomputed data, so that the choice of compression level is a trade-off between CPU use and the size of the precomputed data. Parameters for this figure are $N_{\text{side}} = 2048$, $L = 3N_{\text{side}}$, $m = 0$, and the initial chunk size 32 columns.

sion after three levels reduces the memory bus traffic and size of precomputed data by about 40%, at the cost of some extra CPU instructions. Note that the brute-force codes may simply be seen as the limit of zero levels of compression.

4. IMPLEMENTATION & RESULTS

4.1. Technology

The Wavemoth library is organized in a core part and an auxiliary part. The core is primarily written in C and contains the routines for performing spherical harmonic transforms. The auxiliary shell around the core is written as a Python package, and is responsible generating the precomputed data using the butterfly compression algorithm, as well as the regression and unit tests.

By writing the core in pure C we remain close to the hardware, and make sure the library can be used without Python. C remains the easiest language to call from other languages such as Fortran, C++, Java, Python, MATLAB, and so on. By using Python in the auxiliary support code we accelerate development of the parts that are not performance critical, and make writing tests a pleasant experience. Being able to quickly write up unit tests is an indispensable tool, as it allows optimizing the C code iteratively without introducing bugs. Since individual pieces of the C core is tested, there is both a public API for end-users and a private API that is used from Python to test individual C routines in isolation. Much of the support code is implemented in Cython (Behnel et al. 2011), which bridges the worlds of Python and C.

The C core depends on files containing precomputed data, a Fourier transform library and a BLAS library. For the latter two we use FFTW3 (Frigo & Johnson 2005) and ATLAS (Whaley et al. 2001), respectively. Parts of the Wavemoth core is written using templates in order to generate many slight variations of the same C routine. We use Tempita³, a purely text-oriented templating

language, and find this to be much more convenient for optimizing a computational core than the type-oriented templates of C++. During the precomputations, we use the open source Fortran 77 library ID⁴ to compute the Interpolative Decomposition, and libpsht to generate the associated Legendre functions.

Unlike libpsht, we have not focused on portability, and Wavemoth is only tested on 64-bit Linux with the GCC compiler on Intel-platform CPUs. Computational cores are written using SSE intrinsics and 128-bit registers. More work is needed for optimal performance on the latest Intel micro-architecture, which support 256-bit registers, or on non-Intel platforms. Beyond that, we expect no hurdles in improving portability.

4.2. Benchmarks

We include benchmarks for two different systems with different memory bandwidth, as Wavemoth’s performance is deeply influenced by this aspect of the hardware. Figure 4 presents benchmarks taken on a 64-core 2.27 GHz Intel Xeon X7560 (Nehalem micro-architecture), which has a compute-to-bandwidth ratio of about 45:1. Figure 5 presents benchmarks taken on a 48-core 2.2 GHz AMD Opteron 6174. The compute-to-bandwidth ratio is in this case about 64:1, significantly worse than the Intel system⁵. The consequence is that butterfly compression gives less of an advantage, with only about four times speedup over libpsht at $L = 4096$, compared to the corresponding six times speedup achieved on the Intel system. In the case of ten simultaneous transforms, libpsht achieves a very consistent 2x speedup which Wavemoth is not able to fully match, as most of our tuning effort has been on the single transform path.

The highest tested accuracy of $\epsilon = 10^{-13}$ for the Legendre transforms was chosen because current codes using the HEALPix grid only agree to this accuracy on high resolutions (Reinecke 2011).

An important aspect of the systems for our purposes is the non-uniform memory access (NUMA). On each system, the CPU cores are grouped into eight nodes, and the RAM chips evenly divided between the nodes. Each CPU only have direct access to RAM chips on the local node, and must go through a CPU interconnect bus to access other RAM chips. For consistent performance we need to ensure that Wavemoth distributes the precomputed data in such a way that each CPU finds the data it needs in its local RAM chips. In the benchmarks we always use a whole number of nodes, so that computation power and memory bandwidth scale together. The exception is benchmarks using a single core, but in those cases, Wavemoth’s precomputed data fits in cache anyway.

Table 1 list the sizes of the precomputed data. To balance bandwidth and CPU requirements as described in Section 3.4, the precomputation code takes a parameter ρ , specifying the cost of floating point operations

⁴ <http://cims.nyu.edu/~tygert/software.html>

⁵ The Intel system supports transfer of 13 billion numbers per second and has theoretical peak compute power 580 GFLOPS, using all 64 cores. The AMD system supports transfer of 6.5 billion numbers per second and has theoretical peak compute power of 422 GFLOPS, using all 48 cores. All numbers refer to double precision floating point.

³ <http://pythonpaste.org/tempita/>

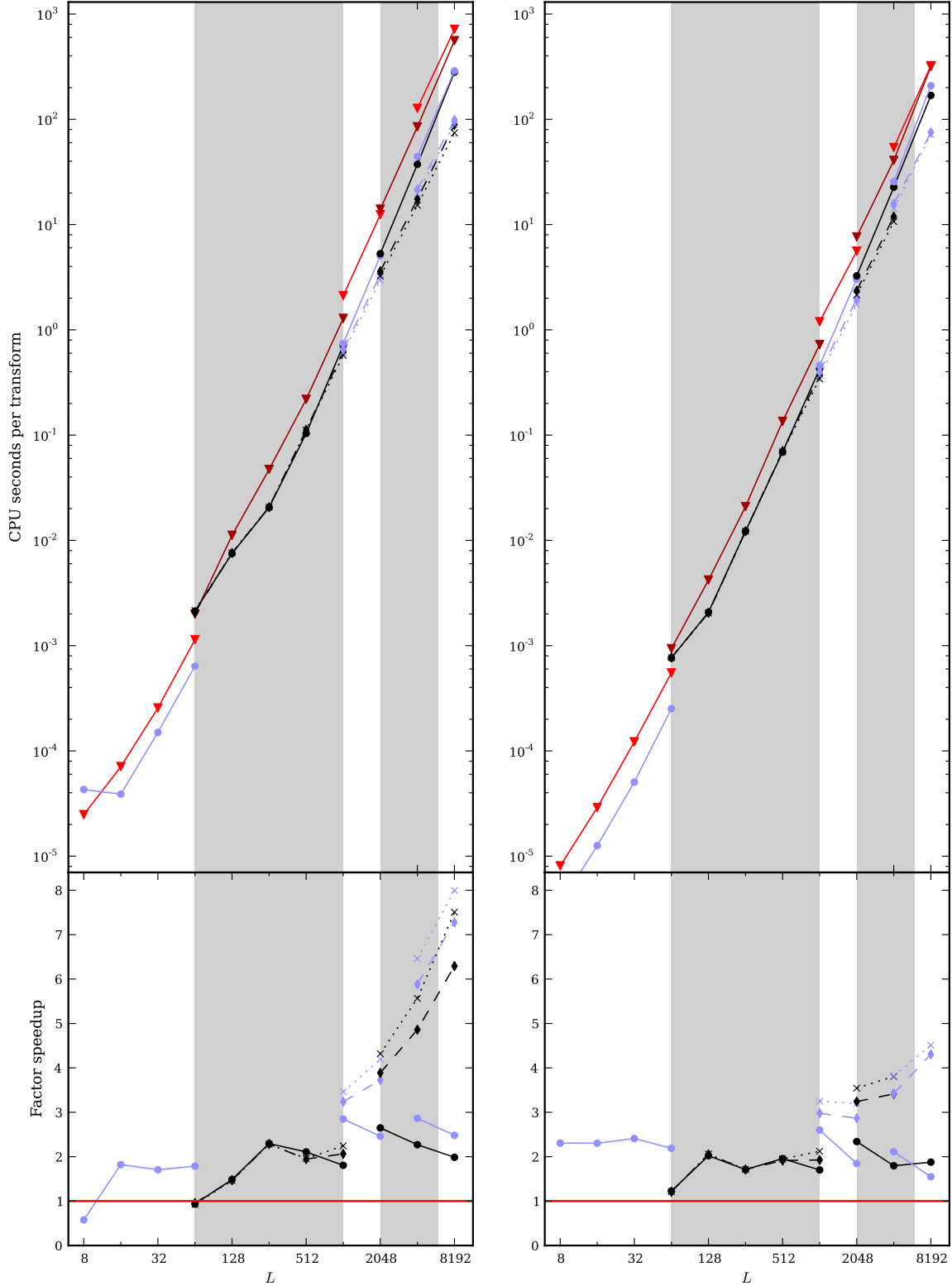


Figure 4. Benchmarks for full SHTs performed on the Intel system. The left pane shows timings for a single transform, the right for ten simultaneous transforms. We scale up the number of CPU cores together with the resolution. Each pane is divided into four partially overlapping segments corresponding to 1, 8, 16, 32, and 64 CPU cores, respectively (indicated by white/gray backgrounds and changes in line colors). The lipsht code (red triangles) is compared to Wavemoth (blue/black) with no compression (solid, circles), compression with precision 10^{-13} (dashed, diamonds) and compression with precision 10^{-8} (dotted, crosses). In each case we use a HEALPix grid with resolution $N_{\text{side}} = L/2$. Note for instance how both codes suffer from parallelization overhead at the transition from one to eight cores, but that lipsht suffers less and catches up with Wavemoth. For a single transform at high resolutions, the situation is the contrary, with Wavemoth parallelizing better at the jump from 16 to 32 cores and from 32 to 64 cores. We repeated each benchmark multiple times both with and without HyperThreading, and report the fastest wall clock time achieved multiplied with the number of CPU cores used and divided by the number of simultaneous transforms. Some 32-core timings for ten simultaneous transforms at $L = 8192$ could not be obtained due to memory limitations. The load time of the precomputed data from the hard drive is not included.

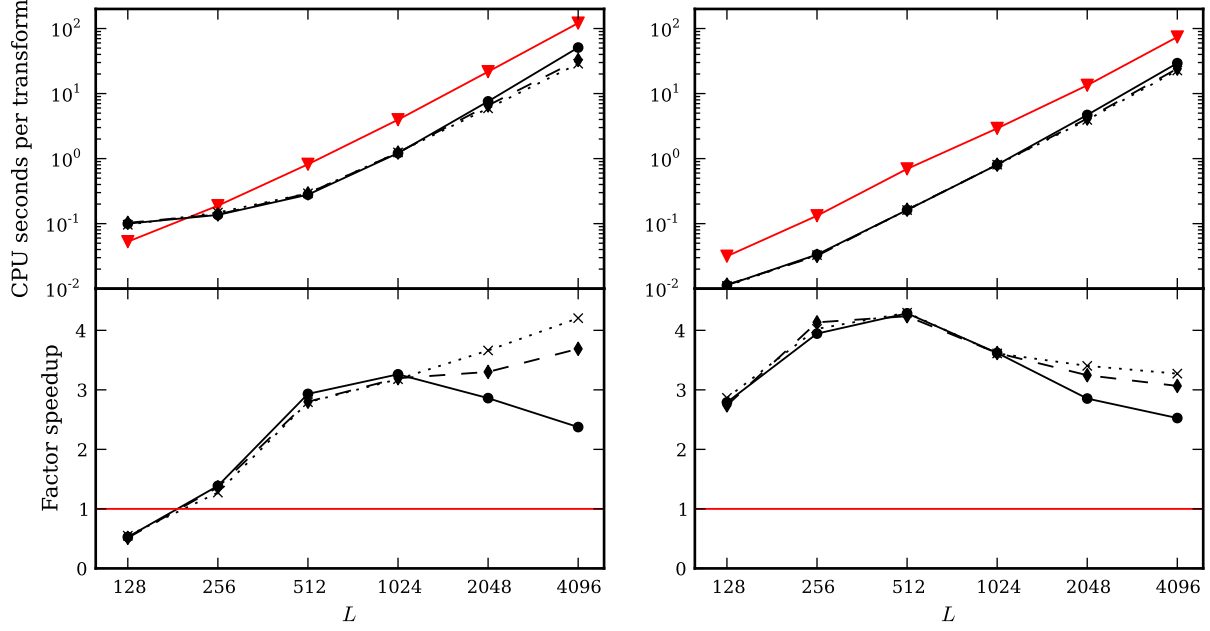


Figure 5. Benchmarks for full SHTs performed on the AMD system, using all 48 CPU cores. The libpsht code (red triangles) is compared to Wavemoth (blue) with no compression (solid, circles), compression with precision 10^{-13} (dashed, diamonds), compression with precision 10^{-8} (dotted, crosses). Left pane shows a single transform and the right pane ten simultaneous transforms. In each case we use a HEALPix grid with resolution $N_{\text{side}} = L/2$. The large speedup in the range $L = 256..1024$ is in part due to Wavemoth scaling better to all 48 cores, and is closer to a 2x speedup when using fewer cores. We repeated each benchmark multiple times, and report the fastest wall clock time achieved multiplied with the number of CPU cores used and divided by the number of simultaneous transforms.

Table 1
Size of precomputed data

L	No comp.	Intel ($\rho = 7.5$)		AMD ($\rho = 18$)		Precomputation time (CPU minutes)
		Tol. 10^{-13}	Tol. 10^{-8}	Tol. 10^{-13}	Tol. 10^{-8}	
32	130 KiB	—	—	—	—	0.02
64	496 KiB	—	—	—	—	0.03
128	2.0 MiB	2.0 MiB	2.0 MiB	1.9 MiB	1.9 MiB	0.22
256	8.0 MiB	8.0 MiB	8.0 MiB	7.1 MiB	7.1 MiB	2.6
512	27 MiB	174 MiB	187 MiB	27 MiB	27 MiB	7.4
1024	102 MiB	937 MiB	988 MiB	102 MiB	170 MiB	12
2048	389 MiB	6.0 GiB	5.8 GiB	4.4 GiB	4.3 GiB	90
4096	1.5 GiB	38 GiB	35 GiB	28 GiB	27 GiB	536
8192	5.8 GiB	212 GiB	208 GiB	—	—	4380

Note. — The precomputation time quoted is the wall time taken to compute at tolerance 10^{-13} on the Intel system, multiplied by the number of CPU cores used. We use 1 core for $L = 32$, and then scale up gradually to 64 cores at $L = 8192$. The precomputed data is saved to a network file system.

Table 2
Samples of numerical accuracy

L	No compression	Tolerance 10^{-13}	Tolerance 10^{-8}
8	8.6e-16	—	—
16	1.4e-15	—	—
32	2.7e-15	—	—
64	5.8e-15	—	—
128	1.2e-14	—	—
512	5.1e-14	4.7e-14	1.9e-09
1024	1.3e-13	8.9e-14	2.4e-09
2048	2.7e-13	1.7e-13	3.1e-09
4096	6.4e-13	3.3e-13	3.7e-09
8192	2.2e-12	6.6e-13	4.2e-09

Note. — In each case, the transform of a single Gaussian sample is compared against libpsht double precision results.

in the bandwidth-intensive butterfly matrix application stage relative to the cost of floating point operations in the CPU-intensive brute-force Legendre transform stage. The parameter was then tuned for the single-transform case for $L = 4096$, resulting in optimal choices of $\rho = 7.5$ on the Intel system and $\rho = 18$ on the AMD system. Performing the precomputations scales as $O(L^3)$. In the case of no compression, we still store the precomputed quantities necessary for the Legendre recurrence relations in memory, as described in the appendix. Loading this data from memory is not necessarily faster than computing it on the fly, but doing so saved some development time.

All methods involved are numerically stable and well understood, so we do not include a rigorous analysis of numerical accuracy. Table 2 lists the relative error from transforming a single set of standard Gaussian coefficients per configuration. We use the relative error

$$\epsilon = \sqrt{\frac{\sum_{i=1}^{N_{\text{pix}}} (x_i - y_i)^2}{\sum_{i=1}^{N_{\text{pix}}} x_i^2}}, \quad (24)$$

where x_i denote the result of libpsht and y_i the result of our code. The discrepancies in the no-compression, high- L cases are due to using a different recurrence for the associated Legendre functions, as described in Appendix A.2. As we did not compare with higher precision results, it is not clear whether it is our code, libpsht, or both, that loose precision with higher resolution. Note that the input data to the butterfly compression is generated using libpsht.

4.3. Higher resolutions

Due to memory constraints we have not gone to higher resolutions than $L \sim 8000$. Instead, we provide estimates for the number of required floating point operations. Tygert (2010) provide similar estimates, but focus on the behavior for the Legendre transform for single m rather than the full SHT.

At each resolution, we compress Λ_m^{odd} for 20 different m , and fit the cost estimate

$$\hat{c}_m = \alpha + \sum_{p=0}^2 \beta_p m \log(1+m)^p \quad (25)$$

by least squares minimization in the parameters α, β_0, β_1 and β_2 . The final cost is then estimated by

$$\hat{c}_{\text{total}} = 2 \sum_{m=0}^L \hat{c}_m, \quad (26)$$

since Λ_m^{even} and Λ_m^{odd} has almost identical behavior. The results can be seen in Figure 2. For $L \sim 130000$, the butterfly algorithm requires only 1% of the arithmetic operations of a brute force transform. The size of the precomputed data at this resolution is around 45 TiB in double precision, although this can be reduced by using the hybrid approach of Section 3.4.

At low resolutions, the algorithm is bound by the $O(L^3)$ operations of the brute-force Legendre transform. At high resolutions, the $O(L^2 \log^2 L)$ trajectory is clearly a better fit than the $O(L^2 \log L)$ scaling conjectured by Tygert (2010). Note that the numerical evidence presented in Tygert (2010) show that the average k increases

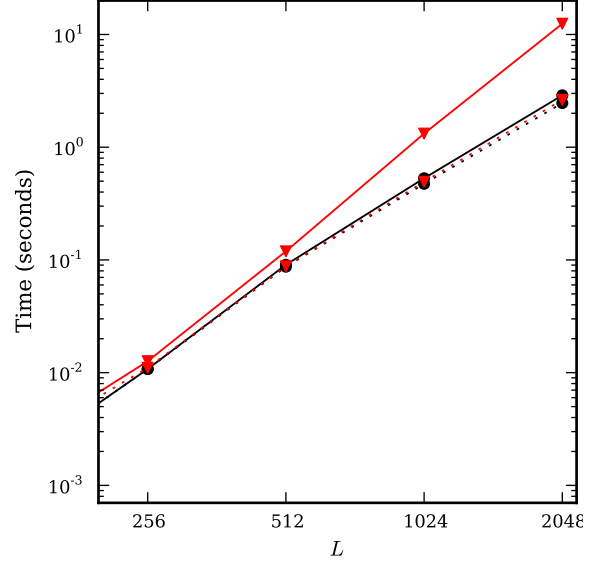


Figure 6. Comparison of Wavemoth (black circles) with the algorithm of Mohlenkamp (1999) as implemented in libftsh (red triangles), with accuracy 10^{-13} (solid) and 10^{-8} (dotted). Both codes are run on a single core. Only the Legendre transform part is benchmarked, as libftsh does not implement the full SHT. Wavemoth uses a HEALPix grid with $2L - 1$ rings, while libftsh uses a Gaussian grid with $2L$ rings. The placement of the rings should make little difference to the performance of either code.

monotonically with m , so it may indeed be the case that the rank property is not fully satisfied, or only satisfied conditional on m . The benchmark results of Tygert (2010) seem to be in agreement with the $O(L^2 \log^2 L)$ hypothesis as well.

4.4. Comparison with other fast SHT algorithms

A widely known scheme for fast SHTs is the $O(L^2 \log^2 L)$ transform of Healy et al. (2003), implemented in SpharmonicKit. It algebraically expresses a Legendre transform of degree L as a function of two Legendre transforms of degree $L/2$, resulting in a divide-and-conquer scheme similar to the FFT algorithms. Unfortunately, the scheme is inherently numerically unstable, and special stabilization steps must be incorporated. Also, it is restricted to equiangular grids, so that it can not be used directly with the HEALPix or GLESP grids. Wiaux et al. (2006) benchmarks SpharmonicKit against the original HEALPix implementation (pre 2.20) and find that it is almost three times slower at $L = 1024$. Keep in mind that libpsht, used in present releases of HEALPix, is about twice as fast as the original HEALPix implementation. Considering the above, we stop short of a direct comparison between Wavemoth and SpharmonicKit. Note that while SpharmonicKit achieves much higher accuracy of an SHT round-trip than HEALPix does, this is an effect of the different sampling grids being used, not of the computational method, and it is straightforward to extend the Wavemoth code to use the same grid as SpharmonicKit.

Mohlenkamp (1999) uses a matrix compression technique similar to the one employed in this paper, which is independent of the pixel grid chosen. A matrix related to the Λ of the present paper is locally approximated by truncated trigonometric series. The resulting SHT algo-

rithm scales as $O(L^{5/2} \log L)$. As shown in Figure 6, the code behaves very similarly to our code at medium resolution, as long as one does not require too much numerical accuracy. The size of the precomputed data is also of the same order, sometimes half and sometimes double that of Wavemoth’s data.

Note that libtsh appears to have potential for optimization for modern platforms, and this should be taken into account when comparing the algorithms. Due to its age, libtsh makes assumptions about 32-bit array sizes which prevents comparison at higher resolutions without porting libtsh to 64-bit. The libtsh code contains an implementation of the Legendre transforms only, and not of the full spherical harmonic transforms. It should be straightforward to modify Wavemoth to use libtsh for its Legendre transforms in order to perform full SHTs using this algorithm.

The compression scheme of Mohlenkamp (1999) appears to be very competitive for low accuracy transforms, but less so if higher precision is needed. It may be fruitful to hybridize the algorithms of Tygert (2010) and Mohlenkamp (1999) and use both together to compress a single matrix. Even if that does not work, one can simply use whichever performs best for a given m .

5. DISCUSSION

There is significant potential in speeding up spherical harmonic transforms beyond the codes in popular use today. We achieved a 2x speedup at low and medium resolutions simply due to restructuring how the brute-force computations are done, and believe there is potential for even more speedup if time is spent on profiling and micro-optimization. In particular, our code is under-optimized for multiple simultaneous transforms.

At the highest resolutions in practical use in cosmology today, $L \sim 4000$, use of the butterfly compression is borderline. On the one hand, it does yield an additional 2x speedup; potentially much more if one needs less accuracy. On the other hand, it requires between 30 and 40 GiB of precomputed data in memory, and the transportation of that data over the memory bus for every set of transforms. The result is a delicate balance between bandwidth and achieved speedup; for every number stored in the precomputed data, one might save 40 arithmetic operations, but then again computation is

much cheaper than accessing system memory on present-day computer architectures.

In Section 3.3, we note the existence of interpolation schemes that cut the necessary sample points for brute-force codes by two thirds in the case of the HEALPix grid; although performing the interpolation step does not come for free. It seems that the speedup from such interpolation alone could be the same order as what the butterfly algorithm achieves for the current needs of CMB research. The advantage is that it does not require nearly as much precomputed data, and is so much less architecture-dependent and easier to micro-optimize. In going forward we therefore anticipate spending more effort on direct interpolation schemes and less effort on matrix compression. For resolutions higher than those needed in CMB analysis, matrix compression schemes seem like the most mature option at the moment.

We have not discussed spin-weighted spherical harmonic transforms, which are crucial to analyzing the polarization properties of the CMB. However, Kostelec et al. (2000) and Wiaux et al. (2007) describe how the transform of a polarized CMB map can be reduced to three scalar transforms. This would additionally help amortize the memory bus transfer of the precomputed data. Alternatively, it may be possible to compress the spin-weighted spherical harmonic operators.

We consider Wavemoth an experimental code for the time being, and spherical harmonic analysis has been left out. This was done purely to save implementation time, and we know of no obstacles to implementing this using the same methods. The code also lacks support for MPI parallelization, although we expect adding such support to be straightforward. The only inter-node communication requirement is a global transpose of $q_m(z_k)$ between the Legendre transforms and the Fourier transforms.

The author thanks S. K. Næss, H. K. Eriksen, M. Tygert, M. Reinecke and M. Mohlenkamp for useful discussions, and M. Omang and F. Hansen for lending the benchmark hardware. The author is funded by European Research Council grant StG2010-257080. The benchmark hardware is funded by the Norwegian Defence Estates Agency and the Research Council of Norway.

APPENDIX

IMPLEMENTATION DETAILS

Applying the compressed matrix representation to a vector

On modern computers, the primary bottleneck is often to move data around. Fundamental design decisions were made with this in mind. Looking at the compressed representations of \mathbf{A} in Section 3.2, the immediate algorithm that comes to mind for computing $\mathbf{A}\mathbf{x}$ or $\mathbf{A}^T\mathbf{x}$ is the breadth-first approach: First compute $\mathbf{S}_1\mathbf{x}$, then permute the result, then compute $\mathbf{S}_2(\mathbf{P}_1\mathbf{S}_1\mathbf{x})$, and so on. However, this leads to storing several temporary results for longer than they need to, since the rightmost permutations are very local permutations, and only the leftmost permutation is fully global. Therefore we traverse the data dependency tree set up by the permutations in a depth-first manner. The advantage of this approach is that it is *cache oblivious* when transforming a few vectors at the time. That is, it automatically minimizes data movement for any cache hierarchy, whereas breadth-first traversal will always drop to the memory layer that is big enough to hold the entire set of input vectors. Note that for transforming many maps at the same time, cache-size dependent blocking should be implemented in addition, but we have stopped short of this. Like Tygert (2010), we also do the compression during precomputation depth-first, which ensures that, per m , memory requirements go as $O(L \log L)$ even though computation time goes as $O(L^2)$.

The core computation during tree traversal is to apply the interpolative matrices, e.g., $\tilde{\mathbf{T}}\mathbf{x}$ or $\tilde{\mathbf{T}}^T\mathbf{x}$. Keep in mind

that the k -by- n matrix $\tilde{\mathbf{T}}$ contains the k -by- k identity matrix in a subset of its columns; making use of this is important as it roughly halves the storage size and FLOP count. Given an ID $\mathbf{T} = \mathbf{T}^{(k)}\tilde{\mathbf{T}}$, we can freely permute the rows of $\tilde{\mathbf{T}}$, simply by permuting the columns of $\mathbf{T}^{(k)}$ correspondingly. We do this during precomputation to avoid the unordered memory usage pattern of arbitrary permutations. Instead, we can simply filter the input or output vectors into the part that hits the identity sub-matrix and the part that hits the dense sub-matrix.

Efficient code for Legendre transforms

As mentioned in Section 3.4, it is necessary to balance the amount of precomputed data to the memory bandwidth, so code is required to apply the residual blocks in \mathbf{R} to vectors without actually storing \mathbf{R} in memory. This means computing a cropped version of the Legendre transform,

$$q'(z_j) = \sum_{k=k_{\text{start}}}^{k_{\text{stop}}} \tilde{P}_{m+2k+t}^m(z_j) a_{\ell m}, \quad (\text{A1})$$

where $t = 0$ for the even transforms and $t = 1$ for the odd transforms. To compute \tilde{P}_ℓ^m we use a relation that jumps two steps in ℓ for each iteration (Tygert 2010):

$$\begin{aligned} \tilde{P}_{\ell+2}^m(z) &= \frac{z^2 - d_\ell^m}{c_\ell^m} \tilde{P}_\ell^m(z) - \frac{c_{\ell-2}^m}{c_\ell^m} \tilde{P}_{\ell-2}^m(z) \\ &\equiv (z^2 + \alpha_\ell^m) \beta_\ell^m \tilde{P}_\ell^m(z) + \gamma_\ell^m \tilde{P}_{\ell-2}^m(z), \end{aligned} \quad (\text{A2})$$

with

$$c_\ell^m = \sqrt{\frac{(\ell - m + 1)(\ell - m + 2)(\ell + m + 1)(\ell + m + 2)}{(2\ell + 1)(2\ell + 3)^2(2\ell + 5)}}$$

and

$$d_\ell^m = \frac{2\ell(\ell + 1) - 2m^2 - 1}{(2\ell - 1)(2\ell + 3)}.$$

This recurrence relation requires five arithmetic operations per iteration, as opposed to a more widely used relation which takes one step in ℓ and only needs four arithmetic operations per step (see, e.g., Press et al. 2007). However, since Λ^{even} and Λ^{odd} may have different columns in the residual blocks of their compressed representations, relation (A2) is a better choice in our case.

For each block in \mathbf{R} we precompute α_ℓ^m , β_ℓ^m and γ_ℓ^m , as well $\tilde{P}_{k_{\text{start}}}^m(z)$ and $\tilde{P}_{k_{\text{start}}+1}^m(z)$ for each z for initial conditions. Note that $\tilde{P}_\ell^m(z)$ in parts of its domain take values so close to zero that they can not be represented in IEEE double precision. However, in these cases $\tilde{P}_\ell^m(z)$ is always increasing in the direction of increasing ℓ , so we can simply increase k_{start} correspondingly. In fact, we follow lipshst and assume that the dynamic range of the input data is small enough, within each m , that values of $\tilde{P}_\ell^m(z)$ smaller than 10^{-30} in magnitude can safely be neglected. As far as possible we group together six and six columns with the same k_{start} and k_{stop} , for reasons that will soon become clear.

For an efficient implementation, the first important point is to make sure the number of loads from cache into CPU registers is balanced with the number of floating-point operations. The second is to make sure there are enough independent floating-point operations in flight simultaneously, so that operations can be pipelined. Thus,

- for performing a single transform with one real and one imaginary vector, the values of \tilde{P}_ℓ^m should never need to leave the CPU registers. Rather, we fuse equation (A1) and equation (A2) in the core loop. For multiple simultaneous transforms we save \tilde{P}_ℓ^m to cache, but make sure to process in small batches that easily fit in L1 cache.
- we process for several z_j simultaneously. This amortizes the register loads of α_ℓ^m , β_ℓ^m and γ_ℓ^m . It also ensures that there are multiple independent chains of computation going on so that pipelining works well.

In the single transform case with one real and one imaginary vector, we do the full summation for six z_j at the time (when possible). The allocation of the 16 available 128-bit registers, each holding two double-precision numbers, then becomes three registers for \tilde{P}_ℓ^m , three for $\tilde{P}_{\ell-2}^m$, three for the auxiliary data α_ℓ^m , β_ℓ^m and γ_ℓ^m , six accumulation registers for $q'(z_j)$, and one work register. The z_j^2 values are, perhaps counter-intuitively, read again from cache in each iteration, which conserves three registers and thus enables processing six z_j in each chunk instead of only four without register spills. Finally, when the time comes for multiplying \tilde{P}_ℓ^m with $a_{\ell m}$, the auxiliary data is no longer needed, leaving room for loading $a_{\ell m}$.

On the Intel Xeon system, the routine performs at 6.46 GFLOP/s per core (71% of the theoretical maximum) when benchmarked on all the Legendre transforms necessary for a full SHT across 32 cores. The effect of instruction

pipelining is evident; reducing the number of columns processed in each iteration from six to four reduces performance to 5.69 GFLOP/s (63%), and when only processing two columns at the time, performance is only 4.28 GFLOP/s (47%).

We skip the details for the multiple transform case, but in short, it involves the same sort of blocking performed for matrix multiplication, including repacking the input data in blocks. Goto & van de Geijn (2008) provide an excellent introduction to blocking techniques. In this case the performance is 5.60 GFLOP/s (62%) per core when performing the Legendre transforms necessary for ten simultaneous SHTs.

The considerations above guided the choice of loop structure, which was then implemented in pure C using SSE intrinsics. We did not spend much time on optimization, so there should be room for further improvements, in particular for the multiple-transform path.

Data layout

The butterfly compression algorithm naturally leads to the following code organization for spherical harmonic synthesis:

1. Since each m is processed independently, we request input in m -major ordering. Also, for multiple simultaneous transforms, the coefficients of each map are interleaved, which is optimal both for the butterfly algorithm and the brute-force cropped Legendre transforms. In most places, the real and complex parts of the input can be treated as two independent vectors, since \mathbf{A} is a real matrix.
2. Compute all $q_m(z_j)$ into a 2D array. Since each m is processed independently, this ends up in m -major ordering, like the input.
3. While transposing the $q_m(z_j)$ array into ring-major ordering, phase-shift and wrap around the coefficients, and perform FFTs on each ring. Rings must be processed in small batches in order to avoid loading cache lines multiple times.

A temporary work buffer with size of the same order as the input and output is used for $q_m(z_j)$. An in-place code should be feasible with the use of an in-place transpose.

A drawback compared to brute-force codes is that $q_m(z_j)$ needs to first be written to and then read from main memory. Here, `libpsht` is instead able to employ blocking, so that a few rings at the time are completely processed before moving on. Our benchmarks do however indicate that this is not a big problem in practice. Also, for cluster parallelization using MPI, it would be natural to follow S²HAT (Hupca et al. 2010; Szydlarski et al. 2011) in distributing the input data by m and the output data by rings, which also leads to a global transpose operation.

Wavemoth stores the output maps in interleaved order, since FFTW3 is able to deal well with such transforms. The `libpsht` code is able to support any output ordering, although stacked, non-interleaved maps are slightly faster, so that is the ordering we use for `libpsht` in the benchmarks.

REFERENCES

- Behnel, S., Bradshaw, R., Citro, C., Dalcin, L., Seljebotn, D. S., & Smith, K. 2011 *Computing in Science & Engineering*, 13, 2
- Cheng, H., Gimbutas, Z., Martinsson, P. G., & Rokhlin, V. 2005 *SIAM J. Sci. Comput.*, 26, 4
- Doroshkevich, A. G., Naselsky, P. D., Verkhodanov, O. V., et al. 2005, *Int. J. Mod. Phys. D*, 14, 275
- Dutt, A., Gu, M., & Rokhlin, V. 1996 *SIAM J. Numer. Anal.*, 33, 5
- Eriksen, H. K., Jewell, J. B., Dickinson, C., Banday, A. J., Górski, K. M., & Lawrence, C. R. 2008 *ApJ*, 676, 1
- Frigo, M., & Johnson, S. G. 2005 *Proceedings of the IEEE*, 93, 2
- Goto, K., & van de Geijn, R. 2008 *ACM Trans. Math. Softw.*, 34, 3
- Górski, K. M., Hivon, E., Banday, A. J., Wandelt, B. D., Hansen, F. K., Reinecke, M., & Bartelmann, M. 2005 *ApJ*, 622, 2
- Healy, D. M., Rockmore, D. N., Kostelec, P. J., & Moore, S. 2003 *Journal of Fourier Analysis and Applications*, 9, 4
- Hupca, I.O., Falcou J., Grigori L., & Stomp R. 2010, INRIA Technical Report, No. RR-7409, arXiv:1010.1260
- Jakob-Chien, R., & Alpert, B. K. 1997 *Journal of Computational Physics*, 136, 2
- Kostelec, P. J., Maslen, D. K., Jr., D. M. H., & Rockmore, D. N. 2000 *Journal of Computational Physics*, 162, 2
- Kunis, S., & Potts, D. 2003 *Journal of Computational and Applied Mathematics*, 161, 1
- Martinsson, P. G., & Rokhlin, V. 2007 *SIAM J. Sci. Comput.*, 29, 3
- McEwen, J. D., & Wiaux, Y. 2011 *Signal Processing, IEEE Transactions on*, 59, 12
- Michielssen, E., & Boag, A. 1996 *IEEE Trans. Antennas Propag.*, 44, 8
- Mohlenkamp, M. J. 1999 *Journal of Fourier Analysis and Applications*, 5, 2
- O’Neil, M., Woolfe, F., & Rokhlin, V. 2010 *Applied and Computational Harmonic Analysis*, 28, 2
- Press, W. H., Teukolsky, S. A., Vetterling, W. T., & Flannery, B. P. 2007 *Numerical Recipes* (3rd ed.; New York, Cambridge University Press)
- Reinecke, M. 2011 *A&A*, 526, A108
- Rokhlin, V., & Tygert, M. 2006 *SIAM J. Sci. Comput.*, 27, 6
- Suda, R., & Takami, M. 2002, *Mathematics of Computation*, 71, 238
- Szydlarski M., Esterie P., Falcou J., Grigori, L., Stomp R. (2011), INRIA technical report, No. RR-7635, arXiv:1106.0159
- Tygert, M. 2008 *Journal of Computational Physics*, 227, 8
- Tygert, M. 2010 *Journal of Computational Physics*, 229, 18
- Whaley, R. C., Petitet, A., & Dongarra, J. 2001 *Parallel Computing*, 27, 1-2
- Wiaux, Y., Jacques, L., Vielva, P., & Vanderghelynst, P. 2006 *ApJ*, 652, 1
- Wiaux, Y., Jacques, L., & Vanderghelynst, P. 2007 *Journal of Computational Physics*, 226, 2
- Yarvin, N., & Rokhlin, V. 1999 *SIAM J. Numer. Anal.*, 36, 2